Updated Calibrated Model for the Prediction of Molecular Frontier Orbital Energies and Its Application to Boron Subphthalocyanines

Devon P. Holst, Pascal Friederich, Alán Aspuru-Guzik, and Timothy P. Bender*

ABSTRACT: A diverse range of computational methods have been used to calibrate against available data and to compare against the correlation for the prediction of frontier orbital energies and optical gaps of novel boron subphthalocyanine (BsubPc) derivatives and related compounds. These properties are of fundamental importance to organic electronic material applications and development, making BsubPcs ideal candidates in pursuit of identifying promising materials for targeted applications. This work employs a database of highly accurate experimental data from materials produced and characterized in-house. The models presented herein calibrate these properties with R^2 values > 0.95. We find that computationally inexpensive semiempirical methods such as PM6 and PM7 outperform most density functional theory methods for calibration. We are excited to share these results with the field as it empowers the community to determine key physical properties of BsubPcs with confidence using free software and a standard laptop prior to the arduous synthesis and purification thereof. This study is a follow up to our previous work calibrating PM3, RM1, and B3LYP-6-31G(d), which used a smaller set of BsubPc derivatives at a past point when less data were available.

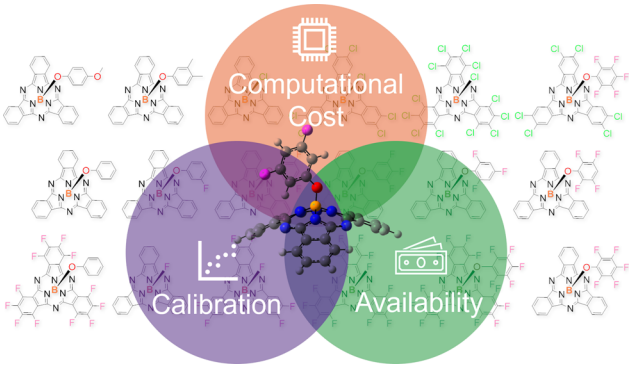

1. INTRODUCTION

Phthalocyanines (Pcs) are well-known planar aromatic macrocycles with bridging sp^2 nitrogen atoms between four repeating isoindoline units. Pc macrocyclic formation can be templated around most metals and metalloids with a variety of ortho-substituted aromatic phthalic compounds, resulting in coordination of the metal atom within the central cavity of the macrocycle.[1] The metal atom precursor used for the templating reaction is typically a metal or metalloid halide with varying degrees of Lewis acidity. Depending on the metal or metalloid halide used for Pc formation, additional moieties may be bound to the metal or metalloid via the remaining moietie(s) in the axial position(s), as shown in Figure 1. When a trivalent boron Lewis acid is used with the precursor phthalonitrile, a nonplanar, bowl-shaped macrocycle with three isoindoline units and C_{3v} symmetry known as boron subphthalocyanine (BsubPc) is uniquely formed. Coordination of boron within the macrocycle cavity forms the only example of a subPc. The macrocyclic structure and the bonding nature of boron stress the BsubPc macrocycle and geometrically conform it into a bowl shape versus all Pc macrocycles, which are planar. A BsubPc is less conjugated than a Pc and therefore has a blue-shifted absorption maximum in the range of 550 nm compared to the greater than 700 nm absorption maxima of Pcs.

The aforementioned structural and electronic features endow Pcs and BsubPcs with unique optoelectronic properties,

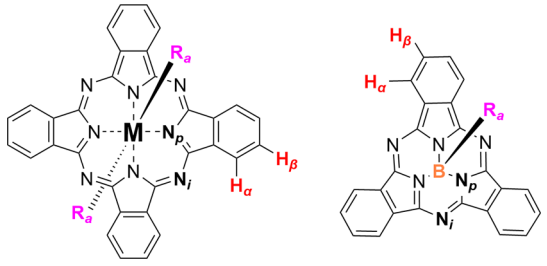

Figure 1. Pc (Left) and BsubPc (right) molecular structure where M is a metal or metalloid atom, R_a is the moieties in the axial positions, N_p is one of the pyrrole nitrogens, N_i is one of the imine nitrogens, and X_α and X_β are substituents in the periphery, which are both the periphery of the Pc and BsubPc. More specifically, X_α denotes a substituent in one of the alpha positions and X_β denotes a substituent in one of the beta positions. Note: some Pcs have only one axial moiety depending on the valency of the templating metal/metalloid atom.

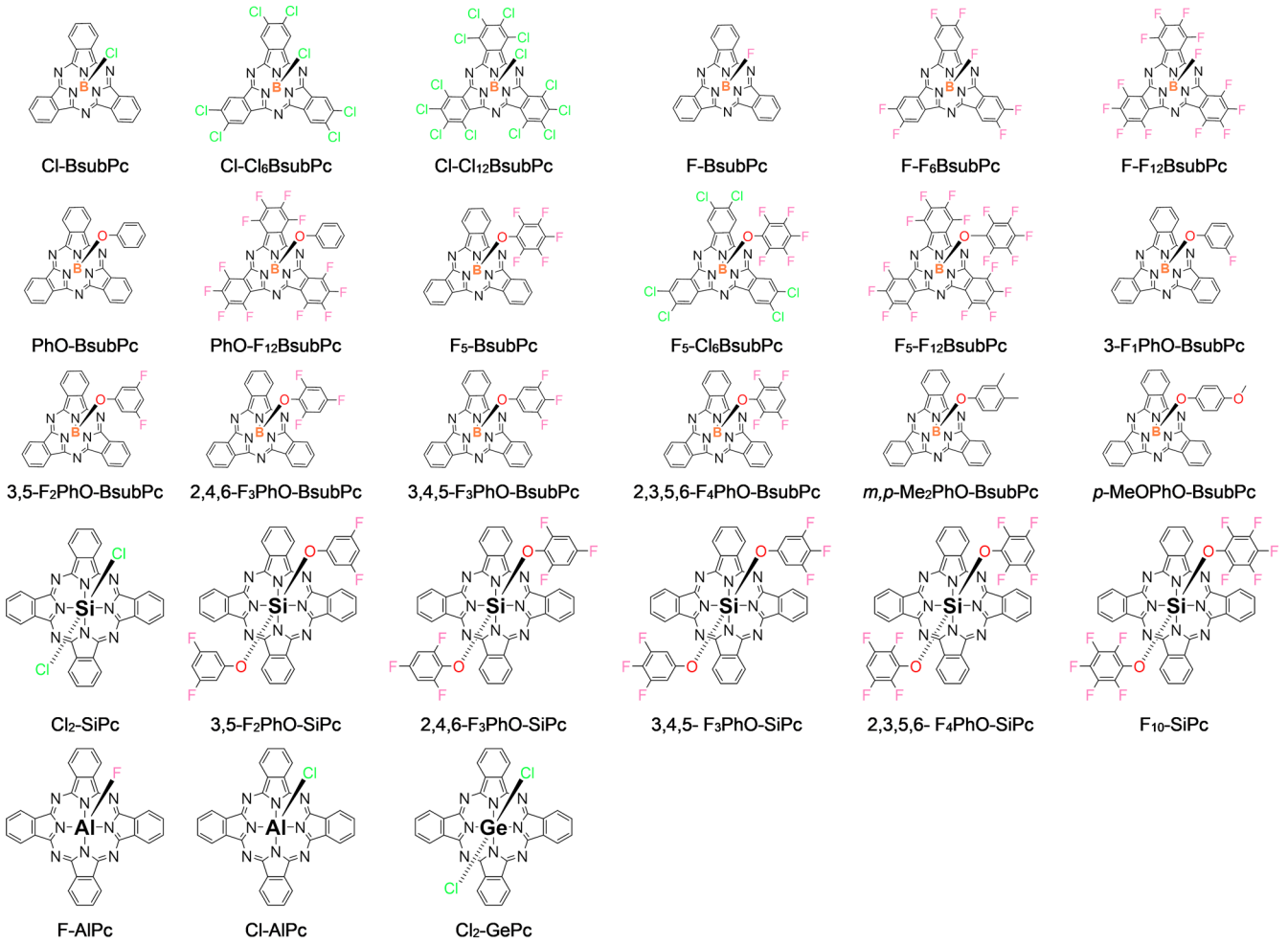

Figure 2. Molecular structures and abbreviations of the compounds investigated in this study.

which has led researchers to study and validate the efficacy of their use in a variety of applications such as but not limited to organic solar cells (OSCs),[2−5] organic light-emitting diodes,[2,6,7] organic field-effect transistors,[8,9] hydrogen evolution photocathodes,[10,11] and fluorescence imaging.[12,13] The success of materials for these applications relies on the energies of frontier molecular orbitals. For example, in an OSC, the difference in energy of the highest occupied molecular orbital (HOMO) of the electron donor and the lowest unoccupied molecular orbital (LUMO) of the electron acceptor dictates the open-circuit voltage of the device and a small offset between the HOMO and LUMO of donor and acceptor materials at the interphase of an OSC is necessary for exciton dissociation. As such, a novel material with inappropriate frontier orbital energies may undergo significant synthetic efforts to produce the material with sufficient purity and scale for testing only to realize that the material was destined for failure. Therefore, a method to accurately screen materials for these key properties prior to a synthetic undertaking is desirable to prevent fruitless synthetic efforts and increase the rate at which materials of high impact are produced.[14−17]

In a world that needs sustainable materials, Pcs and BsubPcs are suitable, as their synthesis is simple[18,19] and they have a low embedded energy[20] and long-term stability under operating conditions.[21,22] As an example, BsubPcs have been shown to have particular interest due to their use in a reasonable efficient OSC as affordable materials and their unusual versatility, being able to function as either of the two necessary active layers and replace fullerenes as electron acceptors in OSCs.[23,24]

The Pc and BsubPc family of semiconductors has been shown to be well suited for HOMO/LUMO energy tuning. The number of possible materials and therefore possible HOMO/LUMO energies grow exponentially as each of the following synthetic factors is considered: incorporation of different core metals or metalloids, functionalization of the metal or metalloid (the axial position), functionalization of the macrocycle (the periphery), and the recently reported possibility of alloying of these materials.[3,4] Considering this, it is probable that materials with higher performance in the aforementioned applications are yet to be discovered. This is currently an active area of research; however, the synthesis, purification, and implementation of these materials into a device to assess their performance are often arduous processes. As such, it is desirable to be able to accurately screen a wide variety of derivatives prior to their synthesis to identify promising candidates prior to synthetic and engineering undertakings.

Our previous 2011 publication[25] investigating the rapid screening of the frontier orbital energies of BsubPcs used the semiempirical methods PM3[26] and RM1.[27] A density functional theory (DFT) method was also employed and was found to correlate experimental and computed values worse than the semiempirical methods tested. Our work also showed that substitutions in the peripheral positions are 2−29 times more

Table 1. Frontier Orbital Energies and Band Gap of the Macrocycles in This Study[a]

compounds and data references[b]	compound abbreviations	film		solution (toluene)		solution (DCM)		solution (DMSO)	
		E_{HOMO}/IE_{UPS} (eV)	average E_{HOMO}/IE_{UPS} (eV)	E_{LUMO} (eV)[c]	$E_{gap,opt}$ (eV)[d]	E_{LUMO} (eV)[c]	$E_{gap,opt}$ (eV)[d]		
1[65]	Cl-BsubPc	5.76[e]	−5.76	−3.66	2.1				
2[66]	Cl−Cl_6BsubPc	−6.30[e] /−6.23[e]	−6.27	−4.26	2.01[f]				
3[66,67]	Cl−Cl_{12}BsubPc	−6.3	−6.3	−4.36	1.94[f]				
4[65]	F-BsubPc	−5.58[e]	−5.58	−3.48	2.1				
5[66]	F−F_6BsubPc	−6.30[e] /−6.37[e]	−6.34	−4.24	2.10[f]				
6[66]	F−F_{12}BsubPc	−6.57[e] /−6.61[e]	−6.59	−4.56	2.03[f]				
7[25,68]	PhO-BsubPc	−5.46/−5.65	−5.56	−3.42	2.14	−3.42	2.14		
8[25]	PhO-F_{12}BsubPc	−6.61	−6.61			−4.49	2.12		
9[25,68,69]	F_5-BsubPc	−5.86/−5.95	−5.91	−3.77	2.14	−3.77	2.14		
10[25]	F_5−Cl_6BsubPc	−6.18	−6.18			−4.06	2.12		
11[25]	F_5−F_{12}BsubPc	−6.65	−6.65			−4.54	2.11		
12[68]	3-F_1PhO-BsubPc	−5.68	−5.68	−3.54	2.14				
13[68]	3,5-F_2PhO-BsubPc	−5.69	−5.69	−3.55	2.14				
14[68]	2,4,6-F_3PhO-BsubPc	−5.54	−5.54	−3.40	2.14				
15[68]	3,4,5-F_3PhO-BsubPc	−5.76	−5.76	−3.62	2.14				
16[68]	2,3,5,6-F_4PhO-BsubPc	−5.76	−5.76	−3.62	2.14				
17[25]	*m,p*-Me_2PhO-BsubPc	−5.42	−5.42			−3.28	2.14		
18[25]	*p*-MeOPhO-BsubPc	−5.42	−5.42			−3.28	2.14		
19[70]	Cl_2-SiPc	−5.7	−5.7	−3.93	1.77				
20[71]	3,5-F_2PhO-SiPc	−5.8	−5.8	−4.02	1.78				
21[71]	2,4,6-F_3PhO-SiPc	−5.4	−5.4	−3.62	1.78				
22[71]	3,4,5- F_3PhO-SiPc	−5.9	−5.9	−4.12	1.78				
23[71]	2,3,5,6- F_4PhO-SiPc	−5.7	−5.7	−3.93	1.77				
24[70]	F_{10}-SiPc	−5.7	−5.7	−3.97	1.73				
25[72]	F-AlPc	−4.7	−4.7					−2.89	1.81
26[70,72]	Cl-AlPc	−5.7	−5.7	−3.93	1.77			−3.92	1.78
27[70]	Cl_2-GePc	−5.8	−5.8	−4.04	1.76				

[a]All HOMO measurements were taken from films of the macrocycles using UPS from the same instrument. [b]Identifiers as outlined in Table S1 of the Supporting Information. [c]$E_{LUMO,Opt} = IE_{UPS} + E_{Gap,Opt}$. [d]In all cases, $E_{Gap,Opt}$ was determined from the onset of the absorbance spectra. [e]New to this work. [f]Redetermined using the onset of absorption.[66]

impactful to the HOMO/LUMO energy levels of these materials than axial functionalization. Also shown, there can be an influence of the axial derivatization but is dependent on the degree of electron-withdrawing character of the equatorial substituents. This provided insights into a methodology whereby axial functionalities could be incorporated to alter properties such as solubility and solid-state arrangement without significantly impacting desirable HOMO/LUMO energies. This model was limited to 7 BsubPcs for experimental validation, and many other BsubPcs were considered after the calibration was complete. With the increasing availability of access to computer clusters, the implementation of DFT for the rapid screening of many possible materials has become feasible with methods that are known to be more accurate than the DFT method employed by our 2011 study.

We present herein a more broadly applicable and experimentally validated model for assessing HOMO/LUMO energies of BsubPcs. This was enabled by the growth of our laboratory's data set and an increased access to computational resources. This model includes a larger set of compounds (27 compounds, Figure 2) with absorption and UPS data that are experimentally valid. A performance assessment of the modernized PM6 and PM7 semiempirical methods as well as a matrix of nine DFT functionals with three basis sets is presented. We identify which method is best suited for accuracy, calibration, and computational cost in pursuit of accelerated materials development. We then identify a method we believe is currently the best balance of these factors for the rapid screening of BsubPcs by their band gap and frontier orbital energies.

We hope this work highlights a relatively straightforward way for anyone with a database of material properties and access to basic computing resources to embark on a similar study, calibrating computational models. With a database of consistent experimental data, there need not be difficult computational considerations influencing accuracy, as absolute accuracy is not necessarily impactful after calibration. Many trends in material properties are accurately predicted by simple computational models that are widely available. The accuracy of a calibrated computational model is dictated mostly by the data set used to calibrate, not by the high level of expertise and computational power needed for work at the forefront of computational chemistry. As such, the computational tools available today and access to them offer an extraordinary tool for materials scientists to accelerate research.

2. METHODS

2.1. Method Selection. The DFT calculations of our previous study employed the basis set 6-31G(d). When

moving to a basis set with more basis functions for valence orbitals, we wanted to probe if diffuse and polarization functions were necessary. For this, we decided to use 6-311G, which lacks both diffuse and polarization functions. Adequate results from this calibration indicated that diffuse and polarization functions were not necessary. This led us to conclude our investigation of the Pople basis sets at 6-311G. We wanted to expand our method for Pcs, which have been formed from many heavy elements and require a basis set that has those elements represented. For this broad method, we hypothesized that a larger basis set would be necessary to unify the calibration for such a broad range of materials. This led us to use the def2-TZVPP basis set.

In order to identify an optimal DFT method for calibration, accuracy, and computational cost, we chose nine functionals, which span a variety of DFT models and three basis sets that are known to vary in computational cost and have been used for the Pc family of macrocycles. From this, we generated a matrix of methods (Table 2) for which we modeled each compound, which has experimental data available as points of calibration to the DFT model(s). Hybrid DFT functionals generally perform well for HOMO predictions, while their long-range corrected counterparts generally perform well for the determination of LUMO energies.[28−30]

We investigated one pure generalized gradient approximation (GGA) functional, seven hybrid functionals, and one Ω-tuned range-separated functional. BP86 was chosen as the pure GGA functional as it has been reported to provide accurate Pc geometries when compared to reported crystal structures as well as usefulness in the computation of their frontier orbital energies.[31,32] This includes Becke's 1988 exchange functional[33] and Perdew's 1986 correlation functional.[34] Our hybrid functional selection included multiple variations of the popular Becke three-parameter hybrid functional,[35] which includes B3LYP,[36,37] B3P86,[34] B3PW91,[38−42] and O3LYP.[43] We also utilized two functionals from the Truhlar group (M11[44] and MN15[45]), the 1996 pure functional of Perdew, Burke, and Ernzerhof made into a hybrid functional by Adamo PBE0,[46] and the Ω-tuned range-separated ωB97X-V[47] from the work of Mardirossian and Head-Gordon. The ωB97X-V functional was tuned, such that the tuning factor aligns the HOMO with the IP and the LUMO with the EA. It was found that one tuning parameter aligned both properties. These functionals have also previously been found useful for either BsubPcs or Pcs.[32] We chose 6-31G(d),[48,49] 6-311G,[50−58] and def2-TZVPP,[59,60] as Pople's 6-31G(d) basis set has been implemented for this family of macrocycles,[61] the 6-311G basis set captures the influence of a triple zeta basis set on the performance of a computation and one of the basis sets proposed by Ahlrichs et al. developed at Karlsruhe, which was expected to outperform both of the previous basis sets at the expense of additional computational cost. The goal of the def2-TZVPP basis set was to aim for the greatest accuracy, which we believed would be significantly dependent on polarization functions. We used def2-TZVPP, as def2-TZVP was shown to be useful for Pcs,[32] and we decided that more polarization functions may further increase the accuracy of this method without significantly increasing the computational cost. We also believed that this method may aid in computations involving heavier atom Pcs such as Cl-GePc and aid in expanding the method in the future if desired. Diffuse functions were not considered necessary, as we do not expect long-range interactions in these systems to be significant, and these functions would add significant computational cost.

Table 2. DFT Frontier Orbital Calibration Outcomes for BsubPcs

functional and molecular orbital	6-31G(d) equation of line (eV) and coefficient of determination	6-311G equation of line (eV) and coefficient of determination	Def2TZVPP equation of line (eV) and coefficient of determination
BP86	$E_H^{Exp} = 1.1974E_H^{BP86} + 0.214$	$E_H^{Exp} = 0.8041E_H^{BP86} - 1.3461$	$E_H^{Exp} = 1.4104E_H^{BP86} + 1.7043$
HOMO	$R2 = 0.8128$	$R2 = 0.9326$	$R2 = 0.9425$
BP86	$E_L^{Exp} = 1.2078E_L^{BP86} + 0.2542$	$E_L^{Exp} = 0.8397E_L^{BP86} - 0.5492$	$E_L^{Exp} = 1.3471E_L^{BP86} + 1.0956$
LUMO	$R2 = 0.8762$	$R2 = 0.9546$	$R2 = 0.9479$
B3LYP	$E_H^{Exp} = 1.0664E_H^{B3LYP} - 0.0892$	$E_H^{Exp} = 0.7246E_H^{B3LYP} - 1.5103$	$E_H^{Exp} = 1.1984E_H^{B3LYP} + 0.9722$
HOMO	$R2 = 0.865$	$R2 = 0.9412$	$R2 = 0.9516$
B3LYP	$E_L^{Exp} = 1.0488E_L^{B3LYP} - 0.909$	$E_L^{Exp} = 0.7424E_L^{B3LYP} - 1.3459$	$E_L^{Exp} = 1.1578E_L^{B3LYP} - 0.2695$
LUMO	$R2 = 0.9031$	$R2 = 0.9556$	$R2 = 0.9513$
B3P86	$E_H^{Exp} = 1.1083E_H^{B3P86} + 0.8856$	$E_H^{Exp} = 0.739E_H^{B3P86} - 0.9491$	$E_H^{Exp} = 1.2725E_H^{B3P86} + 2.1651$
HOMO	$R2 = 0.8685$	$R2 = 0.9474$	$R2 = 0.9434$
B3P86	$E_L^{Exp} = 1.0717E_L^{B3P86} - 0.1469$	$E_L^{Exp} = 0.7581E_L^{B3P86} - 0.8313$	$E_L^{Exp} = 1.2032E_L^{B3P86} + 0.568$
LUMO	$R2 = 0.9049$	$R2 = 0.9569$	$R2 = 0.9441$
B3PW91	$E_H^{Exp} = 1.1084E_H^{B3PW91} + 0.2658$	$E_H^{Exp} = 0.7423E_H^{B3PW91} - 1.3486$	$E_H^{Exp} = 1.2752E_H^{B3PW91} + 1.4582$
HOMO	$R2 = 0.8654$	$R2 = 0.9468$	$R2 = 0.9428$
B3PW91	$E_L^{Exp} = 1.0728E_L^{B3PW91} - 0.741$	$E_L^{Exp} = 0.7612E_L^{B3PW91} - 1.2501$	$E_L^{Exp} = 1.2054E_L^{B3PW91} - 0.1059$
LUMO	$R2 = 0.9033$	$R2 = 0.9567$	$R2 = 0.9441$
O3LYP	$E_H^{Exp} = 1.1764E_H^{O3LYP} + 0.2103$	$E_H^{Exp} = 0.7758E_H^{O3LYP} - 1.4642$	$E_H^{Exp} = 1.371E_H^{O3LYP} + 1.5328$
HOMO	$R2 = 0.8401$	$R2 = 0.9425$	$R2 = 0.9448$
O3LYP	$E_L^{Exp} = 1.1343E_L^{O3LYP} - 0.5461$	$E_L^{Exp} = 0.7976E_L^{O3LYP} - 1.145$	$E_L^{Exp} = 1.2792E_L^{O3LYP} + 0.1684$
LUMO	$R2 = 0.8903$	$R2 = 0.9526$	$R2 = 0.9465$
M11	$E_H^{Exp} = 1.0114E_H^{M11} + 1.4695$	$E_H^{Exp} = 0.6673E_H^{M11} - 0.6358$	$E_H^{Exp} = 1.0518E_H^{M11} + 1.9538$
HOMO	$R2 = 0.8889$	$R2 = 0.9509$	$R2 = 0.9525$
M11	$E_L^{Exp} = 0.9635E_L^{M11} - 2.5401$	$E_L^{Exp} = 0.6918E_L^{M11} - 2.5161$	$E_L^{Exp} = 1.0107E_L^{M11} - 2.2604$
LUMO	$R2 = 0.9156$	$R2 = 0.9567$	$R2 = 0.9464$
MN15	$E_H^{Exp} = 1.0237E_H^{MN15} + 0.193$	$E_H^{Exp} = 0.6681E_H^{MN15} - 1.482$	$E_H^{Exp} = 1.1549E_H^{MN15} + 1.3055$
HOMO	$R2 = 0.8674$	$R2 = 0.9444$	$R2 = 0.9441$
MN15	$E_L^{Exp} = 1.0045E_L^{MN15} - 1.5565$	$E_L^{Exp} = 0.6985E_L^{MN15} - 1.8424$	$E_L^{Exp} = 1.1178E_L^{MN15} - 0.9656$
LUMO	$R2 = 0.9032$	$R2 = 0.9548$	$R2 = 0.9422$
PBE0	$E_H^{Exp} = 1.1075E_H^{PBE0} + 0.3413$	$E_H^{Exp} = 0.7405E_H^{PBE0} - 1.3055$	$E_H^{Exp} = 1.2827E_H^{PBE0} + 1.5945$
HOMO	$R2 = 0.8629$	$R2 = 0.9442$	$R2 = 0.9417$
PBE0	$E_L^{Exp} = 1.0692E_L^{PBE0} - 0.9278$	$E_L^{Exp} = 0.7602E_L^{PBE0} - 1.3826$	$E_L^{Exp} = 1.2098E_L^{PBE0} - 0.287$
LUMO	$R2 = 0.9004$	$R2 = 0.9549$	$R2 = 0.9418$

To expand upon our previous study[25] utilizing the semiempirical methods PM3[26] and RM1,[27] we also investigated their modern versions, PM6[62] and PM7.[63] To do so, we utilized the Molecular Orbital PACkage (MOPAC), which is conveniently free to academia. The outcomes from these methods are expected to have a broader appeal due to their low computational cost, in contrast to DFT.

2.3. Experimental Data and Characterization by Ultraviolet Photoelectron Spectroscopy. To control for the quality and consistency of experimental data used for this

study, each molecule chosen has been synthesized by our lab and characterized by UPS on the same instrument (Table 1). UPS measurements were performed with a PHI 5500 Multi-Technique system. This was attached to a Kurt J. Lesker multiaccess chamber ultrahigh vacuum cluster tool with a base pressure of $\sim 10^{-9}$ Torr and operated at a pressure of $\sim 10^{-7}$ Torr after the introduction of He. The spectrometer was calibrated using XPS with monochromatic Al Kα ($h\nu$ = 1486.7 eV) according to ISO 15472. Zero on the binding energy scale was referenced to the Fermi level of an Ar^+ sputter-cleaned, Au thin film, in electrical contact with the sample. The energy resolution for UPS measurements was ~135 meV as determined by the width of the Fermi edge of the Ar^+ sputter-cleaned, Au thin film. UPS measurements were performed at a photoelectron takeoff angle of 90° with a −15 V bias applied to the sample. The BsubPcs and Pcs were deposited in a dedicated organic chamber from an alumina crucible transfer arm evaporator cell onto freshly cleaved highly ordered pyrolytic graphite substrates. HOMO energy levels for each molecule were determined from 3 nm thick films.

Throughout the history of our lab, we have collected multiple UPS measurements for some materials. Although these data were collected using the same instrument and methodology, the results vary slightly. We found that E_{HOMO} varied by ± 0.095 eV at most, which occurred when the experiment was re-run for the same material 7 years apart. This small change exemplifies the consistency of UPS measurements and is likely due to a drift in the acquired results between calibrations of the instrument. In all other cases of duplicate data, the difference in the data collected is significantly lower to us, indicating that the method employed is reasonably reproducible for our purposes. For compounds with multiple E_{HOMO} data points, we have used the average of all values in our calibrations to avoid weighting the calibration more heavily on one compound by including each duplicate data point individually. Duplicate data points are listed in Table 1.

2.4. Conformation and Isomer Considerations. The BsubPcs and Pcs modeled are derivatives of symmetric phthalonitriles. As a result, each of BsubPc and Pc is an equatorially symmetric macrocycle and does not require a consideration of equatorial isomers. The phenoxy groups were found to be oriented above an imine nitrogen between two of the isoindoline units aligning with crystal structures that have been reported for these macrocycles. We found that the phenoxy group has two minimum energy points, which we are calling edge-on and face-on (Figure 3). We compared the total energy of each conformation from a B3LYP-6-31G(d) computation in order to determine the global minimum for each phenoxylated compound. The difference in total energy between these two conformations was found to be less than 1 kcal/mol. The lowest energy conformer was not found to be exclusively one of the conformations. Indeed, only 3,5-F_2PhO-BsubPc was found to have an edge-on global minimum energy conformation, while all other phenoxylated BsubPcs were found to have a face-on global minimum energy conformation. The lowest energy conformation was used to determine frontier orbital energies. Conformational total energy data have been included in the Supporting Information (Table S2).

In case of the more flexible Pcs with two axial functional groups, we performed a conformer search based on a combination of metadynamics simulations and semiempirical calculations (GFNn-xTB), using the CREST simulation

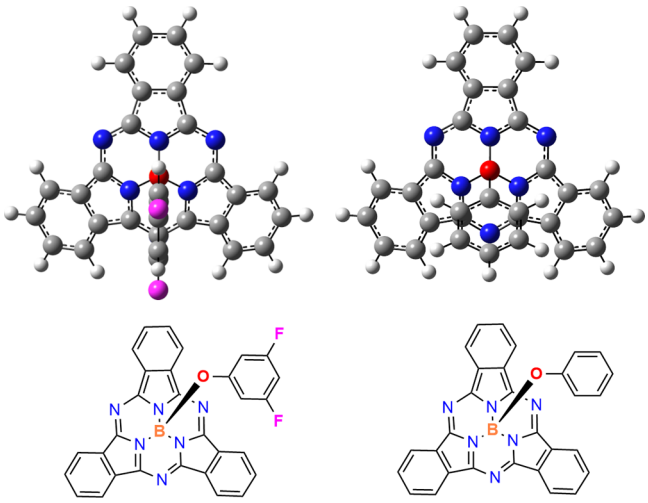

Figure 3. 3,5-F_2PhO-BsubPc in the edge-on conformation (top left) and PhO-BsubPc in the face-on conformation (top right). The corresponding 2D structures are shown below their respective 3D structures.

package.[73] Between four (2,3,5,6-F_3PhO-SiPC) and eight (3,4,5-F_3PhO-SiPC) conformers within an energy window of 6 kcal/mol above the global minimum were found, and the lowest energy conformer was used for further calculations.

2.5. Computational Process. Before submitting any compound for DFT calculations, the structures were generated in Avogadro (https://avogadro.cc) from ChemDraw.mol files and UFF relaxations were performed to generate initial structures. The coordinates of these structures were then used for submission to the Compute Canada SHARCNET cluster running Gaussian 16. For a given functional, the lowest level basis set was first used for geometry optimization followed by subsequent higher-level basis sets. In the case of BsubPcs, this followed the order of 6-31G(d), 6-311G, and finally Def2TZVPP. In this way, a structure closer to a minimum energy was fed into each subsequent higher-level calculation in order to reduce the total CPU time required to complete the calculations. The frontier orbital energies were calculated using the geometry optimized structure for each given functional and basis set combination. As the basis set 6-31G(d) was found to calibrate the worst, Pcs were only modeled using the basis sets 6-311G and def2-TZVPP.

3. RESULTS AND DISCUSSION

3.1. Correlation between Experimental and DFT Predicted Energies. The desire for this work is to accurately predict frontier orbital energies in order to allow for the screening of BsubPcs and Pcs prior to a synthetic effort to synthesize and purify them for use in organic electronics. In this light, an accurate prediction of the energy of frontier orbitals was not considered as important as a strong correlation between experimental and predicted orbital energies (Figures 4–6). As such, R^2 values of a linear least square fit between calculated frontier orbital energies and experimental frontier orbital energies have been given the greatest influence over the recommendation of a method (Tables 2–4). The following tables and figures outline the results of our calibrations.

3.2. Frontier Orbital Energy Calibrations. As expected, the quality of HOMO calibrations between DFT functionals generally increased from pure GGA, to hybrid, and finally to

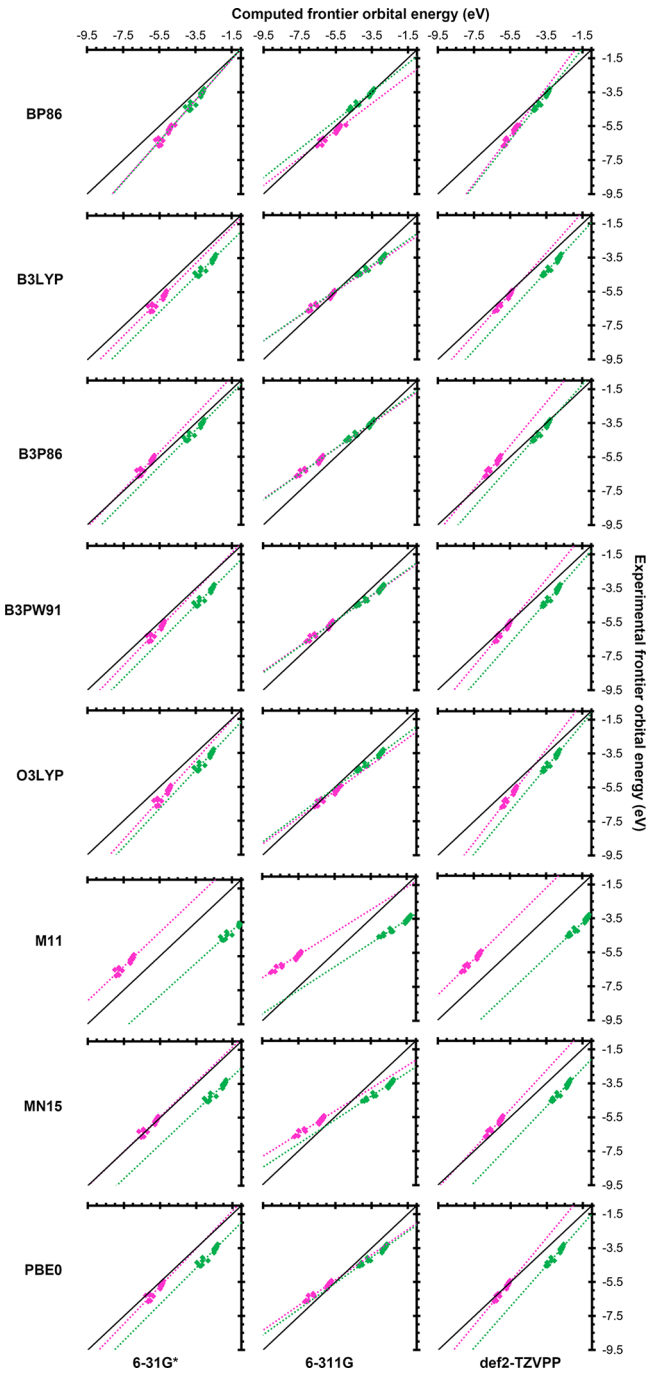

Figure 4. Pair plot of functionals and basis sets calibrated in this study where the *x*-axis is the computed frontier orbital energy ($E_{H/L}^{functional}$) and the *y*-axis is the experimental frontier orbital energy ($E_{H/L}^{Exp}$). HOMO data are displayed as the pink point, and LUMO data are displayed as green points. Dashed lines are included in the same color as their respective data set and represent linear least square fits. The line $y = x$ is included in black as a comparison to a perfect computational model, which requires no calibration. ωB97X-V def2-TZVPP is not included in this pair plot and is discussed separately later. Data sets are available in the Supporting Information.

the Ω-tuned range-separated hybrid functional. This improvement in the quality of the correlation between the pure GGA functional BP86 was significant when the 6-31G(d) basis set was employed whereby an R^2 value of 0.8128 was obtained for BP86 and an R^2 value of 0.8889 and 0.8401 was derived for the best and worst hybrid methods M11 and O3LYP, respectively. This difference in the quality of the calibration was only marginal when the 6-311G basis sets were employed. BP86 with the 6-311G basis set resulted in an R^2 value of 0.9326, while the best and worst calibrations of hybrid DFT functionals were 0.9509 and 0.9412 for M11 and B3LYP, respectively. When the def2-TZVPP basis set was employed, the pure GGA functional BP86 performed on par with its hybrid functional counterparts. BP86 with the def2-TZVPP basis set resulted in an R^2 value of 0.9425, while the best and worst calibrations of a hybrid DFT functional were 0.9525 and 0.9434 with M11 and B3P86, respectively. This leads us to conclude that the basis set is more influential to the calibration of BsubPc HOMO values than the functional.

In line with the HOMO calibrations, the quality of LUMO calibrations between DFT functionals generally increased from pure GGA, to hybrid, and finally to the Ω-tuned range-separated hybrid functional. This improvement in the quality of the correlation between the pure GGA functional BP86 was significant when the 6-31G(d) basis set was employed, whereby an R^2 value of 0.8762 was obtained for BP86 and R^2 values of 0.9156 and 0.8903 were derived for the best and worst hybrid methods M11 and O3LYP, respectively. This difference in the quality of the calibration was only marginal when the 6-311G basis sets was employed. BP86 with the 6-311G basis set resulted in an R^2 value of 0.9546, while the best and worst calibrations of hybrid DFT functionals were 0.9569 and 0.9526 for B3P86 and O3LYP, respectively. When the def2-TZVPP basis set was employed, the pure GGA functional BP86 performed on par with its hybrid functional counterparts. BP86 with the def2-TZVPP basis set resulted in an R^2 value of 0.9479, while the best and worst calibrations of a hybrid DFT functional were 0.9513 and 0.9418 with B3LYP and PBE0, respectively. In line with HOMO calibrations, this leads us to conclude that the basis set is also more influential to the calibration of BsubPc LUMO values than the functional.

Ω-tuned range-separated functionals are known to yield more accurate results for orbital energies compared to conventional functionals.[28,30] During the Ω-tuning process, HOMO and LUMO energies are corrected in a way to correspond to the negative vertical ionization energy (−|IP| or −|EA|), bringing them closer to what is actually measured in experiments. As shown in Figure 5 and Table 3, the procedure works well for experimental HOMO energies, but less so for experimental LUMO energies, which are predicted to be shallower than those observed experimentally. We suspect that the reason for this is not a failure of the range separated functionals, but rather the fact that the experimental LUMO energies are determined by adding the optical energy gap to the measured HOMO energy. When mimicking this procedure in DFT (Figure 5), the quantitative agreement between predicted LUMOs and measured LUMOs reduces significantly. Overall, we find rather high correlation coefficients for HOMO energies predicted by range-separated functionals (R^2 = 0.9677), while for LUMO energies, some of the DFT functionals ($R^2 \sim 0.95$, see next section) perform better than the range-separated functionals (R^2 = 0.9398).

3.3. DFT basis Set and Functional Choice. The basis set 6-311G is the clear winner out of the basis sets employed in this study. It often outperforms def2-TZVPP at a fraction of the computational cost. 6-31G(d) performed relatively poorly compared to 6-311G and def2-TZVPP when used with a

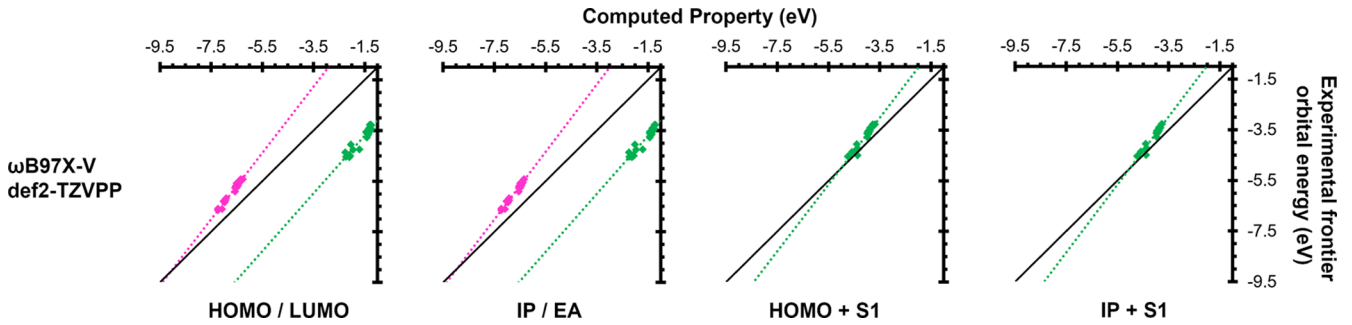

Figure 5. Pair plot of the outcomes from computations employing the Ω-tuned range-separated functional ωB97X-V with the basis set def2-TZVPP where the x-axis is the computed frontier orbital energy ($E_{H/L}^{functional}$) and the y-axis is the experimental frontier orbital energy ($E_{H/L}^{Exp}$). HOMO data are displayed as pink points, and LUMO data are displayed as green points. Dashed lines are included in the same color as their respective data set and represent linear least square fits. The line $y = x$ is included in black as a comparison to a perfect computational model, which requires no calibration. Data sets are available in the Supporting Information.

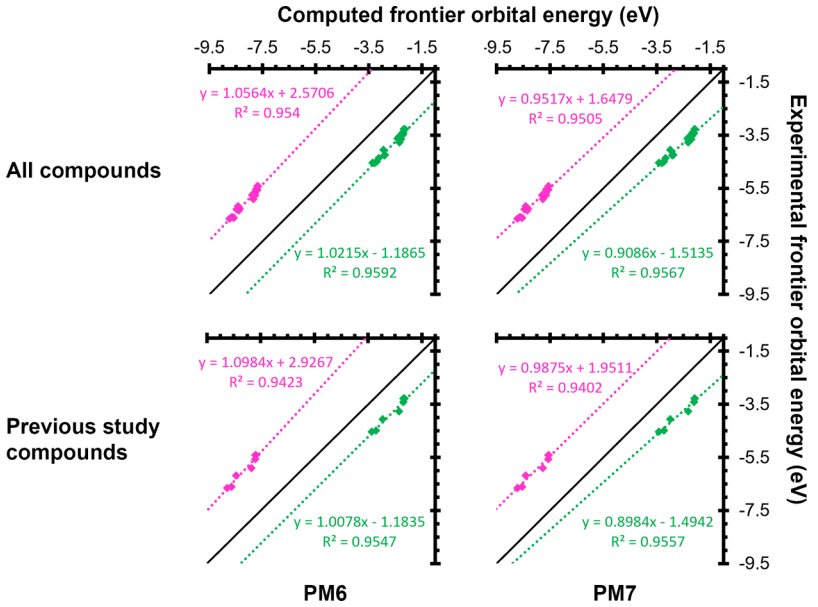

Figure 6. Pair plot of semiempirical methods calibrated in this study where the x-axis is the computed frontier orbital energy ($E_{H/L}^{functional}$) and the y-axis is the experimental frontier orbital energy ($E_{H/L}^{Exp}$). For comparison, the calibrations were also conducted with the same set of compounds used in our previous study.[25]

Table 3. Frontier Orbital Calibration Outcomes for BsubPcs from the Computations Employing the Ω-Tuned Range-Separated Functional ωB97X-V with the Basis Set def2-TZVPP

ωB97X-V def2-TZVPP method	HOMO equation of line (eV) and coefficient of determination	LUMO equation of line (eV) and coefficient of determination
HOMO/LUMO	$E_H^{Exp} = 1.3093E_H^{Calc} + 2.817$	$E_L^{Exp} = 1.1418E_L^{Calc} - 1.9937$
	$R^2 = 0.9677$	$R^2 = 0.8933$
IP/EA	$E_H^{Exp} = 1.333E_H^{Calc} + 2.9794$	$E_L^{Exp} = 1.1466E_L^{Calc} - 1.9931$
	$R^2 = 0.9668$	$R^2 = 0.9133$
HOMO + S1		$E_L^{Exp} = 1.3169E_L^{Calc} + 1.5988$
		$R^2 = 0.9398$
IP + S1		$E_L^{Exp} = 1.3403E_L^{Calc} + 1.6996$
		$R^2 = 0.9394$

hybrid functional. def2-TZVPP was found to be beneficial when using a pure GGA functional.

The choice of hybrid functional was not found to have a significant influence over the quality of the calibration. Hybrid functionals were found to generally calibrate better than the pure GGA functional examined.

3.4. Computational Cost. To compare the computational cost of a given basis set, we compared the time for a geometry optimization of the Cl-BsubPc with the B3LYP functional and the same initial geometry. We chose Cl-BsubPc, as this BsubPc does not contain significant degrees of freedom such as that of an axial phenolic moiety, which was found to at times cause the geometry optimization to get stuck temporarily in a local minimum before finding the global minimum energy geometry. Geometry optimizations using the B3LYP functional with the 6-31G(d), 6-311G, and def2-TZVPP basis sets took 9 min and 9.7 s, 4 min and 43.6 s, and 1 h 51 min and 53 s respectively. This indicates that 6-311G is the most computationally inexpensive basis set. When contrasting the computational cost with the calibration results of these studies, 6-311G is in our opinion the optimal DFT basis set for the rapid screening of BsubPcs using a calibrated method. While slightly increasing the accuracy in HOMO prediction, the Ω-tuning step in case

Table 4. Semiempirical Frontier Orbital Calibration Outcomes for BsubPcs from This Study as Well as Our Previous Study

<!−Col Count:3--> >method	HOMO equation of line (eV) and coefficient of determination	LUMO equation of line (eV) and coefficient of determination
PM6[a]	$E_H^{Exp} = 1.0564E_H^{PM6} + 2.5706$	$E_L^{Exp} = 1.0215E_L^{PM6} - 1.1865$
	$R^2 = 0.954$	$R^2 = 0.9592$
PM7[a]	$E_H^{Exp} = 0.9517E_H^{PM7} + 1.6479$	$E_L^{Exp} = 0.9086E_L^{PM7} - 1.5135$
	$R^2 = 0.9505$	$R^2 = 0.9567$
RM1[b]	$E_H^{Exp} = 1.007E_H^{RM1} + 1.834$	$E_L^{Exp} = 0.888E_L^{RM1} - 1.723$
	$R^2 = 0.961$	$R^2 = 0.968$
PM3[b]	$E_H^{Exp} = 1.105E_H^{PM3} + 3.067$	$E_L^{Exp} = 1.012E_L^{PM3} - 1.118$
	$R^2 = 0.951$	$R^2 = 0.967$
RM1[c]	$E_H^{Exp} = 0.9715E_H^{RM1} + 1.5385$	$E_L^{Exp} = 0.8575E_L^{RM1} - 1.8157$
	$R^2 = 0.9453$	$R^2 = 0.9537$
PM3[c]	$E_H^{Exp} = 1.069E_H^{PM3} + 2.7521$	$E_L^{Exp} = 0.9832E_L^{PM3} - 1.2147$
	$R^2 = 0.9405$	$R^2 = 0.9549$
PM6[d]	$E_H^{Exp} = 1.0984E_H^{PM6} + 2.9267$	$E_L^{Exp} = 1.0078E_L^{PM6} - 1.1835$
	$R^2 = 0.9423$	$R^2 = 0.9547$
PM7[d]	$E_H^{Exp} = 0.9875E_H^{PM7} + 1.9511$	$E_L^{Exp} = 0.8984E_L^{PM7} - 1.4942$
	$R^2 = 0.9402$	$R^2 = 0.9557$

[a]Calibrated using all BsubPcs included in this study. [b]From our previous calibration publication.[25] [c]Calibrated using the previous study's computational results and this study's experimental data set. [d]Calibrated using the same BsubPcs as our previous calibration publication.

of the range separated functionals adds additional complexity as well as significant computational cost. Given the relatively small added value compared to conventional functionals, we do not recommend the use of Ω-tuned range-separated functionals for large-scale screening studies for this class of materials. However, they might add some certainty in computational predictions when applied to promising candidates before synthesis and experimental characterization. Furthermore, they might be more reliable for molecules, which significantly differ from the calibration data set, and for which thus the calibration might not be suitable.

3.5. Correlation between Experimental and Semiempirical Predicted Energies. To compare the semiempirical methods used in our previous calibration publication to their newer versions employed in this study, we have included calibrations using the same more limited set of BsubPcs (Figure 6). We find that the newer semiempirical methods PM6 and PM7 calibrate virtually identical to their outdated counterparts (Table 4). RM1 and PM3 calibrate HOMOs slightly better, while PM6 and PM7 were found to calibrate LUMOs slightly better. All of these methods have very low computational cost, and the quality of its calibration enables anyone to predict the frontier orbital energies of BsubPcs. As such, we recommend everyone use any of the investigated semiempirical methods with their respectively reported calibration if predicting the frontier orbital energies of BsubPcs is desired.

3.6. Calibration Barriers. When using semiempirical and DFT methods to compute frontier orbital energies of our set of BsubPcs, the LUMO energies generally calibrate better than the HOMO energies. This outcome suggests that the DFT and semiempirical method's inaccuracy in directly computing LUMO energies is not reflected in the relative difference in computed LUMO energies, allowing for the direct LUMO computation inaccuracy to be overcome by calibration. This highlights the fact that when a high-quality data set for a family of molecules is used to calibrate a model in the way presented, properties that are typically difficult to accurately predict are simplified. Our implementation of the ωB97X-V functional with the def2-TZVPP basis set results in a relatively close direct prediction of the LUMO energy and confirms that this method to quantitatively predict the LUMO by the addition of the computed optical gap to the ionization potential or the HOMO is optimal if a data set for calibration is not available (Figure 5). The pure GGA functional BP86 with the 6-311G basis set resulted in a remarkably accurate direct prediction of LUMO energies, which we anticipate might be a result of error cancellation.

3.7. Calibration of Pcs. Attempts to calibrate a model for the Pcs resulted in a champion correlation coefficient of 0.621 with the M11 functional and the 6-311G basis set (Figure S1). The poor calibration of Pcs is presumably due to the small basis set and changing central metal atoms. This seems to indicate that separate calibrations should be conducted for each different central metal/metalloid atom of a phthalocyanine. Furthermore, our data set for the Pcs is much smaller, inhibiting the calibration efficacy and supporting the idea that a bigger set of experimental data is necessary to conduct calibrations such as that presented herein. The same holds true for more complex functionalizations, for example, with larger aromatic compounds, which might influence the nature of the HOMO and LUMO orbitals and thus make new calibrations necessary. Therefore, we do not propose a calibrated method for the computation of Pc frontier orbital energies.

3.8. Equatorial/Peripheral Substituents and Their Influence on the Methodology. BsubPcs with high degrees of equatorial chlorination were found to be problematic for the calibrations conducted when using the DFT functionals with the 6-31G(d) basis set. Most notably, Cl−Cl_{12}BsubPc was generally the worst outlier in these calibrations. The use of larger basis sets such as 6-311G and def2-TZVPP or semiempirical methods was found to resolve this. This further supports the use of the 6-311G basis set for DFT frontier orbital calculations or any of the investigated semiempirical calculations.

3.9. UV−Vis Calibration. The optical gaps reported herein are taken from previous publications from our group using the onset of the absorption method. Solution UV−vis data were used in all cases due to their availability for all materials modeled and lack of potential solid-state anomalies as observed for F-AlPc[72] and the models inability to capture these characteristics. One of our publications utilized reported optical gaps for F−F_6BsubPc, F−F_{12}BsubPc, Cl−Cl_6BsubPc, and Cl−Cl_{12}BsubPc[66] using a different method to determine the optical gap. For this publication, we have redetermined the optical gap using the onset of the absorption method for data consistency. The number of significant figures varies between 2 and 3 presumably due to the authors' perceived accuracy of picking the onset of absorption. This method is known to result in slight differences when conducted by different people as picking the onset of absorption is not clear but rather something that requires intuition. New optical gap data reported herein are reported to three significant figures in order to align with the majority of data previously published by our group.

The absorption data of PhO-BsubPc and F_5-BsubPc indicate that the effect of solvent on the band gap and thereby the determined LUMO of the materials studied is negligible. As

such, absorption data in both DCM and toluene were used as is without consideration of the influence of the solvent. The negligible influence of the solvent on the absorbance data is likely due to the delocalization of frontier orbitals throughout the macrocycle, preventing the solvent from playing a major role in stabilizing the excited state of the molecules. In other words, the excitation of an electron is significantly stabilized by the conjugated system, thereby reducing the ability of the solvent to play a significant role in its stabilization or lack thereof. If the solvent was a significant source of excited-state stabilization, the difference in dielectric constant between these two solvents would be expected to result in a difference in the absorption spectrum. As both solvents are not hydrogen donors, stabilization through hydrogen bonding was not considered.

Based on our use of UV−vis for the experimental determination of LUMOs and the prevalence of time-dependent methods in the determination of this optoelectronic property, it should be noted that the investigation of time-dependent methods is of interest. Generally, time-dependent DFT (TD-DFT) is employed although semiempirical time-dependent methods are also available[74] but suffer from generally lower accuracy than TD-DFT methods. As accuracy is not necessary for a successful calibration, it is unclear if time-dependent DFT or semiempirical computations would be beneficial. Nevertheless, we are exploring these points to date and will be publishing results of our investigation moving forward.

4. CONCLUSIONS

The calibration conducted herein alleviates the need for computationally expensive frontier orbital energy predictions for BsubPcs as demonstrated by the high correlation coefficients (R^2 > 0.95) when calibrating the semiempirical methods PM6 and PM7. We have updated our previous calibrated DFT method for screening BsubPc frontier orbital energies with a significantly larger experimental data set of BsubPc frontier orbital energies. We employed the Ω-tuned range-separated functional ωB97X-V, which was found to produce the best calibration for HOMO energies (R^2 = 0.9677) of any method employed but fell short of the other functionals and the semiempirical methods for LUMO calibrations. A variety of hybrid functional and basis set combinations were calibrated, and the 6-311G basis set was found to provide good calibrations at a reasonable computational cost compared to the 6-31G(d) and def2-TZVPP basis sets. The 6-31G(d) basis set was found to produce significantly worse calibrations than the 6-311G and def2-TZVPP basis sets. Of the hybrid functionals investigated, the M11 functional was found to calibrate best for HOMOs, while the B3P86 functional was found to calibrate best for LUMOs, although the difference in correlation coefficients was minimal, suggesting that most hybrid functionals are suitable for calibration. Using the same methodology for a set, Pcs was found to result in poor quality calibrations. We do not recommend the use of the Pc calibrations outlined herein. We highly recommend the use of PM6 or PM7 with the calibrated model reported herein and believe that it will be useful in enhancing the rate of development of novel highly functional BsubPcs.

SOFTWARE AND DATA AVAILABILITY

All data used for the calibrations can be obtained in the Supporting Information of this publication. Additional data are available from the authors upon request. ChemDraw was used to build 2D structures, which were imported into Avogadro to perform UFF relaxations and generate initial 3D structures. ChemDraw can be purchased at https://perkinelmerinformatics.com/. Avogadro can be acquired for free at https://avogadro.cc.[64] All DFT calculations except those employing the ωB97X-V functional were conducted using Gaussian 16, which can be purchased through https://gaussian.com/. DFT calculations using the ωB97X-V functional were conducted using Q-Chem version 5.1.1, which can be purchased at https://www.q-chem.com/. MOPAC version 2016 was used for all semiempirical calculations and was obtained for free from http://openmopac.net/. When necessary, conformational searches were conducted using the conformer-rotamer ensemble sampling tool version 2.6 (CREST), which is available at https://github.com/grimme-lab.

ASSOCIATED CONTENT

Supporting Information

The Supporting Information is available free of charge at https://pubs.acs.org/doi/10.1021/acs.jcim.1c01048.

Table of modeled compounds, total energies from the investigation of edge-on and face-on phenol orientation used to determine the minimum energy structure for frontier orbital energy computations, HOMO calibration results of BsubPcs and Pcs using the M11 functional and 6-311G basis set, and experimentally determined (UPS) and computed frontier orbital energies for the calibration of all functionals and basis sets (PDF)

SMILES data for all compounds included in this publication (CSV)

AUTHOR INFORMATION

Corresponding Author

Timothy P. Bender − *Department of Chemical Engineering and Applied Chemistry, University of Toronto, Toronto M5S 3E5, Canada; Department of Chemistry, University of Toronto, Toronto M5S 3H6, Canada; Department of Materials Science and Engineering, University of Toronto, Toronto M5S 3E4, Canada;* orcid.org/0000-0002-6086-7445; Email: tim.bender@utoronto.ca

Authors

Devon P. Holst − *Department of Chemical Engineering and Applied Chemistry, University of Toronto, Toronto M5S 3E5, Canada; Department of Chemistry, University of Toronto, Toronto M5S 3H6, Canada*

Pascal Friederich − *Department of Chemistry, University of Toronto, Toronto M5S 3H6, Canada; Department of Computer Science, University of Toronto, Toronto M5T 3A1, Canada; Institute of Nanotechnology, Karlsruhe Institute of Technology, Eggenstein-Leopoldshafen 76344, Germany;* Present Address: Institute of Theoretical Informatics, Karlsruhe Institute of Technology, Am Fasanengarten 5, 76131 Karlsruhe, Germany

Alán Aspuru-Guzik − *Department of Chemistry, University of Toronto, Toronto M5S 3H6, Canada; Department of Computer Science, University of Toronto, Toronto M5T 3A1,*

Canada; Vector Institute for Artificial Intelligence, Toronto M5G 1M1, Canada; Lebovic Fellow, Canadian Institute for Advanced Research (CIFAR), Toronto M5G 1M1, Canada; orcid.org/0000-0002-8277-4434

Complete contact information is available at: https://pubs.acs.org/10.1021/acs.jcim.1c01048

Notes

The authors declare no competing financial interest.

■ ACKNOWLEDGMENTS

This work was made possible by the facilities of the Shared Hierarchical Academic Research Computing Network (SHARCNET: www.sharcnet.ca) and Compute/Calcul Canada (www.computecanada.ca). We would like to acknowledge the molecular editor and visualizer Avogadro, which was used frequently during this work.[64] This work was enabled by the software Gaussian 16 for most DFT calculations.[75] We would like to acknowledge MOPAC and their generous free availability to academic institutions.

■ REFERENCES

(1) Claessens, C. G.; Hahn, U.; Torres, T. Phthalocyanines: From Outstanding Electronic Properties to Emerging Applications. *Chem. Rec.* **2008**, *8*, 75−97.

(2) Morse, G. E.; Bender, T. P. Boron Subphthalocyanines as Organic Electronic Materials. *ACS Appl. Mater. Interfaces* **2012**, *4*, 5055−5068.

(3) Dang, J. D.; Josey, D. S.; Lough, A. J.; Li, Y.; Sifate, A.; Lu, Z.-H.; Bender, T. P. The Mixed Alloyed Chemical Composition of Chloro-(chloro)n-Boron Subnaphthalocyanines Dictates their Physical Properties and Performance in Organic Photovoltaic Devices. *J. Mater. Chem. A* **2016**, *4*, 9566−9577.

(4) Dang, J. D.; Josey, D. S.; Dang, M. T.; Bender, T. P. Phenoxy-(Chloro)n-Boron Subnaphthalocyanines: Alloyed Mixture, Electron-Accepting Functionality, and Enhanced Solubility for Bulk Heterojunction Organic Photovoltaics. *ACS Omega* **2018**, *3*, 2093−2103.

(5) Tang, C. W. Two-Layer Organic Photovoltaic Cell. *Appl. Phys. Lett.* **1986**, *48*, 183−185.

(6) Plint, T. G.; Lessard, B. H.; Bender, T. P. Doping Chloro Boron Subnaphthalocyanines and Chloro Boron Subphthalocyanine in Simple OLED Architectures Yields Warm White Incandescent-Like Emissions. *Opt. Mater.* **2018**, *75*, 710−718.

(7) Blochwitz, J.; Pfeiffer, M.; Fritz, T.; Leo, K. Low Voltage Organic Light Emitting Diodes Featuring Doped Phthalocyanine as Hole Transport Material. *Appl. Phys. Lett.* **1998**, *73*, 729−731.

(8) Horowitz, G. Organic Field-Effect Transistors. *Adv. Mater.* **1998**, *10*, 365−377.

(9) Yasuda, T.; Tsutsui, T. n-Channel Organic Field-Effect Transistors Based on Boron-Subphthalocyanine. *Mol. Cryst. Liq. Cryst.* **2006**, *462*, 3−9.

(10) Morozan, A.; Bourgeteau, T.; Tondelier, D.; Geffroy, B.; Jousselme, B.; Artero, V. Noble Metal-Free Hydrogen-Evolving Photocathodes Based on Small Molecule Organic Semiconductors. *Nanotechnology* **2016**, *27*, 355401.

(11) Abe, T.; Tobinai, S.; Taira, N.; Chiba, J.; Itoh, T.; Nagai, K. Molecular Hydrogen Evolution by Organic p/n Bilayer Film of Phthalocyanine/Fullerene in the Entire Visible-Light Energy Region. *J. Phys. Chem. C* **2011**, *115*, 7701−7705.

(12) Bernhard, Y.; Richard, P.; Decréau, R. A. Addressing Subphthalocyanines and Subnaphthalocyanines Features Relevant to Ffluorescence Imaging. *Tetrahedron* **2018**, *74*, 1047−1052.

(13) Li, X.; Kim, C.-y.; Lee, S.; Lee, D.; Chung, H.-M.; Kim, G.; Heo, S.-H.; Kim, C.; Hong, K.-S.; Yoon, J. Nanostructured Phthalocyanine Assemblies with Protein-Driven Switchable Photoactivities for Biophotonic Imaging and Therapy. *J. Am. Chem. Soc.* **2017**, *139*, 10880−10886.

(14) Hachmann, J.; Olivares-Amaya, R.; Atahan-Evrenk, S.; Amador-Bedolla, C.; Sánchez-Carrera, R. S.; Gold-Parker, A.; Vogt, L.; Brockway, A. M.; Aspuru-Guzik, A. The Harvard Clean Energy Project: Large-Scale Computational Screening and Design of Organic Photovoltaics on the World Community Grid. *J. Phys. Chem. Lett.* **2011**, *2*, 2241−2251.

(15) Olivares-Amaya, R.; Amador-Bedolla, C.; Hachmann, J.; Atahan-Evrenk, S.; Sánchez-Carrera, R. S.; Vogt, L.; Aspuru-Guzik, A. Accelerated Computational Discovery of High-Performance Materials for Organic Photovoltaics by Means of Cheminformatics. *Energy Environ. Sci.* **2011**, *4*, 4849−4861.

(16) Sokolov, A. N.; Atahan-Evrenk, S.; Mondal, R.; Akkerman, H. B.; Sánchez-Carrera, R. S.; Granados-Focil, S.; Schrier, J.; Mannsfeld, S. C. B.; Zoombelt, A. P.; Bao, Z.; Aspuru-Guzik, A. From Computational Discovery to Experimental Characterization of a High Hole Mobility Organic Crystal. *Nat. Commun.* **2011**, *2*, 437.

(17) Lopez, S. A.; Sanchez-Lengeling, B.; de Goes Soares, J.; Aspuru-Guzik, A. Design Principles and Top Non-Fullerene Acceptor Candidates for Organic Photovoltaics. *Joule* **2017**, *1*, 857−870.

(18) Meller, A.; Ossko, A. Phthalocyaninartige Bor-Komplexe. *Monatsh. Chem.* **1972**, *103*, 150−155.

(19) Kopylovich, M. N.; Kukushkin, V. Y.; Haukka, M.; Luzyanin, K. V.; Pombeiro, A. J. L. An Efficient Synthesis of Phthalocyanines Based on an Unprecedented Double-Addition of Oximes to Phthalonitriles. *J. Am. Chem. Soc.* **2004**, *126*, 15040−15041.

(20) Anctil, A.; Babbitt, C. W.; Raffaelle, R. P.; Landi, B. J. Cumulative Energy Demand for Small Molecule and Polymer Photovoltaics. *Prog. Photovoltaics* **2013**, *21*, 1541−1554.

(21) Josey, D. S.; Nyikos, S. R.; Garner, R. K.; Dovijarski, A.; Castrucci, J. S.; Wang, J. M.; Evans, G. J.; Bender, T. P. Outdoor Performance and Stability of Boron Subphthalocyanines Applied as Electron Acceptors in Fullerene-Free Organic Photovoltaics. *ACS Energy Lett.* **2017**, *2*, 726−732.

(22) Josey, D. S.; Ingram, G. L.; Garner, R. K.; Wang, J. M.; Evans, G. J.; Lu, Z.-H.; Bender, T. P. Outdoor Stability of Chloro-(Chloro)n-Boron Subnaphthalocyanine and Chloro-Boron Subphthalocyanine as Electron Acceptors in Bilayer and Trilayer Organic Photovoltaics. *ACS Appl. Energy Mater.* **2019**, *2*, 979−986.

(23) Garner, R. K.; Dang, M. T.; Dang, J. D.; Bender, T. P. The Mixed Alloyed Chemical Composition of Chloro-(chloro)n-Boron Subnaphthalocyanines Dictates Their Performance as Electron-Donating and Hole-Transporting Materials in Organic Photovoltaics. *ACS Appl. Energy Mater.* **2018**, *1*, 1029−1036.

(24) Verreet, B.; Cnops, K.; Cheyns, D.; Heremans, P.; Stesmans, A.; Zango, G.; Claessens, C. G.; Torres, T.; Rand, B. P. Decreased Recombination Through the Use of a Non-Fullerene Acceptor in a 6.4% Efficient Organic Planar Heterojunction Solar Cell. *Adv. Energy Mater.* **2014**, *4*, 1301413.

(25) Morse, G. E.; Helander, M. G.; Stanwick, J.; Sauks, J. M.; Paton, A. S.; Lu, Z.-H.; Bender, T. P. Experimentally Validated Model for the Prediction of the HOMO and LUMO Energy Levels of Boronsubphthalocyanines. *J. Phys. Chem. C* **2011**, *115*, 11709−11718.

(26) Stewart, J. J. P. MOPAC: A Semiempirical Molecular Orbital Program. *J. Comput. Aided Mol. Des.* **1990**, *4*, 1−103.

(27) Rocha, G. B.; Freire, R. O.; Simas, A. M.; Stewart, J. J. P. RM1: A Reparameterization of AM1 for H, C, N, O, P, S, F, Cl, Br, and I. *J. Comput. Chem.* **2006**, *27*, 1101−1111.

(28) Kar, R.; Song, J.-W.; Hirao, K. Long-Range Corrected Functionals Satisfy Koopmans' Theorem: Calculation of Correlation and Relaxation Energies. *J. Comput. Chem.* **2013**, *34*, 958−964.

(29) Nakata, A.; Tsuneda, T. Density Functional Theory for Comprehensive Orbital Energy Calculations. *J. Chem. Phys.* **2013**, *139*, 064102.

(30) Zhang, G.; Musgrave, C. B. Comparison of DFT Methods for Molecular Orbital Eigenvalue Calculations. *J. Phys. Chem. A* **2007**, *111*, 1554−1561.

(31) Nemykin, V. N.; Sabin, J. R. Profiling Energetics and Spectroscopic Signatures in Prototropic Tautomers of Asymmetric Phthalocyanine Analogues. *J. Phys. Chem. A* **2012**, *116*, 7364−7371.
(32) Colomban, C.; Kudrik, E. V.; Briois, V.; Shwarbrick, J. C.; Sorokin, A. B.; Afanasiev, P. X-ray Absorption and Emission Spectroscopies of X-Bridged Diiron Phthalocyanine Complexes (FePc)2X (X = C, N, O) Combined with DFT Study of (FePc)2X and Their High-Valent Diiron Oxo Complexes. *Inorg. Chem.* **2014**, *53*, 11517−11530.
(33) Becke, A. D. Density-Functional Exchange-Energy Approximation with Correct Asymptotic Behavior. *Phys. Rev. A* **1988**, *38*, 3098−3100.
(34) Perdew, J. P. Density-Functional Approximation for the Correlation Energy of the Inhomogeneous Electron Gas. *Phys. Rev. B: Condens. Matter Mater. Phys.* **1986**, *33*, 8822−8824.
(35) Becke, A. D. Density-Functional Thermochemistry. III. The Role of Exact Exchange. *J. Chem. Phys.* **1993**, *98*, 5648−5652.
(36) Lee, C.; Yang, W.; Parr, R. G. Development of the Colle-Salvetti Correlation-Energy Formula Into a Functional of the Electron Density. *Phys. Rev. B: Condens. Matter Mater. Phys.* **1988**, *37*, 785−789.
(37) Miehlich, B.; Savin, A.; Stoll, H.; Preuss, H. Results Obtained with the Correlation Energy Density Functionals of Becke and Lee, Yang and Parr. *Chem. Phys. Lett.* **1989**, *157*, 200−206.
(38) Perdew, J. P. *Electronic Structure of Solids '91*; Akademie Verlag: Berlin, 1991.
(39) Perdew, J. P.; Chevary, J. A.; Vosko, S. H.; Jackson, K. A.; Pederson, M. R.; Singh, D. J.; Fiolhais, C. Atoms, Molecules, Solids, and Surfaces: Applications of the Generalized Gradient Approximation for Exchange and Correlation. *Phys. Rev. B: Condens. Matter Mater. Phys.* **1992**, *46*, 6671−6687.
(40) Perdew, J. P.; Chevary, J. A.; Vosko, S. H.; Jackson, K. A.; Pederson, M. R.; Singh, D. J.; Fiolhais, C. Erratum: Atoms, Molecules, Solids, and Surfaces: Applications of the Generalized Gradient Approximation for Exchange and Correlation. *Phys. Rev. B: Condens. Matter Mater. Phys.* **1993**, *48*, 4978.
(41) Perdew, J. P.; Burke, K.; Wang, Y. Generalized Gradient Approximation for the Exchange-Correlation Hole of a Many-Electron System. *Phys. Rev. B: Condens. Matter Mater. Phys.* **1996**, *54*, 16533−16539.
(42) Burke, K. J. P. P.; Wang, Y. *Electronic Density Functional Theory Recent Progress and New Directions*; Plenum Press: New York, 1998.
(43) Cohen, A. J.; Handy, N. C. Dynamic Correlation. *Mol. Phys.* **2001**, *99*, 607−615.
(44) Peverati, R.; Truhlar, D. G. Improving the Accuracy of Hybrid Meta-GGA Density Functionals by Range Separation. *J. Phys. Chem. Lett.* **2011**, *2*, 2810−2817.
(45) Yu, H. S.; He, X.; Li, S. L.; Truhlar, D. G. MN15: A Kohn−Sham Global-Hybrid Exchange−Correlation Density Functional with Broad Accuracy for Multi-Reference and Single-Reference Systems and Noncovalent Interactions. *Chem. Sci.* **2016**, *7*, 5032−5051.
(46) Adamo, C.; Barone, V. Toward Reliable Density Functional Methods Without Adjustable Parameters: The PBE0 Model. *J. Chem. Phys.* **1999**, *110*, 6158−6170.
(47) Mardirossian, N.; Head-Gordon, M. ωB97X-V: A 10-Parameter, Range-Separated Hybrid, Generalized Gradient Approximation Density Functional with Nonlocal Correlation, Designed by a Survival-of-the-Fittest Strategy. *Phys. Chem. Chem. Phys.* **2014**, *16*, 9904−9924.
(48) Petersson, G. A.; Bennett, A.; Tensfeldt, T. G.; Al-Laham, M. A.; Shirley, W. A.; Mantzaris, J. A Complete Basis Set Model Chemistry. I. The Total Energies of Closed-Shell Atoms and Hydrides of the First-Row Elements. *J. Chem. Phys.* **1988**, *89*, 2193−2218.
(49) Petersson, G. A.; Al-Laham, M. A. A Complete Basis Set Model Chemistry. II. Open-Shell Systems and the Total Energies of the First-Row Atoms. *J. Chem. Phys.* **1991**, *94*, 6081−6090.
(50) McLean, A. D.; Chandler, G. S. Contracted Gaussian Basis Sets for Molecular Calculations. I. Second Row Atoms, Z=11−18. *J. Chem. Phys.* **1980**, *72*, 5639−5648.
(51) Krishnan, R.; Binkley, J. S.; Seeger, R.; Pople, J. A. Self-Consistent Molecular Orbital Methods. XX. A Basis Set for Correlated Wave Functions. *J. Chem. Phys.* **1980**, *72*, 650−654.
(52) Blaudeau, J.-P.; McGrath, M. P.; Curtiss, L. A.; Radom, L. Extension of Gaussian-2 (G2) Theory to Molecules Containing Third-Row Atoms K and Ca. *J. Chem. Phys.* **1997**, *107*, 5016−5021.
(53) Wachters, A. J. H. Gaussian Basis Set for Molecular Wavefunctions Containing Third-Row Atoms. *J. Chem. Phys.* **1970**, *52*, 1033−1036.
(54) Hay, P. J. Gaussian Basis Sets for Molecular Calculations. The Representation of 3d Orbitals in Transition-Metal Atoms. *J. Chem. Phys.* **1977**, *66*, 4377−4384.
(55) Raghavachari, K.; Trucks, G. W. Highly Correlated Systems. Excitation Energies of First Row Transition Metals Sc−Cu. *J. Chem. Phys.* **1989**, *91*, 1062−1065.
(56) Binning, R. C., Jr.; Curtiss, L. A. Compact Contracted Basis Sets for Third-Row Atoms: Ga−Kr. *J. Comput. Chem.* **1990**, *11*, 1206−1216.
(57) McGrath, M. P.; Radom, L. Extension of Gaussian-1 (G1) Theory to Bromine-Containing Molecules. *J. Chem. Phys.* **1991**, *94*, 511−516.
(58) Curtiss, L. A.; McGrath, M. P.; Blaudeau, J. P.; Davis, N. E.; Binning, R. C.; Radom, L. Extension of Gaussian-2 Theory to Molecules Containing Third-Row Atoms Ga−Kr. *J. Chem. Phys.* **1995**, *103*, 6104−6113.
(59) Weigend, F.; Ahlrichs, R. Balanced Basis Sets of Split Valence, Triple Zeta Valence and Quadruple Zeta Valence Quality for H to Rn: Design and Assessment of Accuracy. *Phys. Chem. Chem. Phys.* **2005**, *7*, 3297−3305.
(60) Weigend, F. Accurate Coulomb-Fitting Basis Sets for H to Rn. *Phys. Chem. Chem. Phys.* **2006**, *8*, 1057−1065.
(61) Yang, Y. J.; Su, Z. M. Structure, Stability, and Aromaticity of M-SubPc (MB, Al, and Ga): Computational Study. *Int. J. Quantum Chem.* **2005**, *103*, 54−59.
(62) Stewart, J. J. P. Optimization of Parameters for Semiempirical Methods V: Modification of NDDO Approximations and Application to 70 Elements. *J. Mol. Model.* **2007**, *13*, 1173−1213.
(63) Stewart, J. J. P. Optimization of Parameters for Semiempirical Methods VI: More Modifications to the NDDO Approximations and Re-Optimization of Parameters. *J. Mol. Model.* **2013**, *19*, 1−32.
(64) Hanwell, M. D.; Curtis, D. E.; Lonie, D. C.; Vandermeersch, T.; Zurek, E.; Hutchison, G. R. Avogadro: an Advanced Semantic Chemical Editor, Visualization, and Analysis Platform. *J. Cheminf.* **2012**, *4*, 17.
(65) Fulford, M. V.; Jaidka, D.; Paton, A. S.; Morse, G. E.; Brisson, E. R. L.; Lough, A. J.; Bender, T. P. Crystal Structures, Reaction Rates, and Selected Physical Properties of Halo-Boronsubphthalocyanines (Halo = Fluoride, Chloride, and Bromide). *J. Chem. Eng. Data* **2012**, *57*, 2756−2765.
(66) Bukuroshi, E.; Vestfrid, J.; Gross, Z.; Bender, T. P. Fluorinated Boron Subphthalocyanines: Lewis Acid Based Templating Chemistry Facilitates Random Halide Exchange, and Fluoride Versus Chloride Affects the Basic Photophysical Properties and the Solid-State Arrangement. *New J. Chem.* **2019**, *43*, 16730−16737.
(67) Castrucci, J. S.; Josey, D. S.; Thibau, E.; Lu, Z.-H.; Bender, T. P. Boron Subphthalocyanines as Triplet Harvesting Materials within Organic Photovoltaics. *J. Phys. Chem. Lett.* **2015**, *6*, 3121−3125.
(68) Sampson, K. L.; Josey, D. S.; Li, Y.; Virdo, J. D.; Lu, Z.-H.; Bender, T. P. Ability To Fine-Tune the Electronic Properties and Open-Circuit Voltage of Phenoxy-Boron Subphthalocyanines through Meta-Fluorination of the Axial Substituent. *J. Phys. Chem. C* **2018**, *122*, 1091−1102.
(69) Helander, M. G.; Morse, G. E.; Qiu, J.; Castrucci, J. S.; Bender, T. P.; Lu, Z.-H. Pentafluorophenoxy Boron Subphthalocyanine As a Fluorescent Dopant Emitter in Organic Light Emitting Diodes. *ACS Appl. Mater. Interfaces* **2010**, *2*, 3147−3152.
(70) Lessard, B. H.; White, R. T.; Al-Amar, M.; Plint, T.; Castrucci, J. S.; Josey, D. S.; Lu, Z.-H.; Bender, T. P. Assessing the Potential Roles of Silicon and Germanium Phthalocyanines in Planar

Heterojunction Organic Photovoltaic Devices and How Pentafluoro Phenoxylation Can Enhance $\pi-\pi$ Interactions and Device Performance. *ACS Appl. Mater. Interfaces* **2015**, *7*, 5076−5088.
(71) Lessard, B. H.; Grant, T. M.; White, R.; Thibau, E.; Lu, Z.-H.; Bender, T. P. The Position and Frequency of Fluorine Atoms Changes the Electron Donor/Acceptor Properties of Fluorophenoxy Silicon Phthalocyanines Within Organic Photovoltaic Devices. *J. Mater. Chem. A* **2015**, *3*, 24512−24524.
(72) Lessard, B. H.; Al-Amar, M.; Grant, T. M.; White, R.; Lu, Z.-H.; Bender, T. P. From Chloro to Fluoro, Expanding the Role of Aluminum Phthalocyanine in Organic Photovoltaic Devices. *J. Mater. Chem. A* **2015**, *3*, 5047−5053.
(73) Grimme, S. Exploration of Chemical Compound, Conformer, and Reaction Space with Meta-Dynamics Simulations Based on Tight-Binding Quantum Chemical Calculations. *J. Chem. Theory Comput.* **2019**, *15*, 2847−2862.
(74) Bartell, L. A.; Wall, M. R.; Neuhauser, D. A Time-Dependent Semiempirical Approach to Determining Excited States. *J. Chem. Phys.* **2010**, *132*, 234106.
(75) Frisch, M. J.; Trucks, G. W.; Schlegel, H. B.; Scuseria, G. E.; Robb, M. A.; Cheeseman, J. R.; Scalmani, G.; Barone, V.; Petersson, G. A.; Nakatsuji, H.; Li, X.; Caricato, M.; Marenich, A. V.; Bloino, J.; Janesko, B. G.; Gomperts, R.; Mennucci, B.; Hratchian, H. P.; Ortiz, J. V.; Izmaylov, A. F.; Sonnenberg, J. L.; Williams; Ding, F.; Lipparini, F.; Egidi, F.; Goings, J.; Peng, B.; Petrone, A.; Henderson, T.; Ranasinghe, D.; Zakrzewski, V. G.; Gao, J.; Rega, N.; Zheng, G.; Liang, W.; Hada, M.; Ehara, M.; Toyota, K.; Fukuda, R.; Hasegawa, J.; Ishida, M.; Nakajima, T.; Honda, Y.; Kitao, O.; Nakai, H.; Vreven, T.; Throssell, K.; Montgomery, J. A., Jr.; Peralta, J. E.; Ogliaro, F.; Bearpark, M. J.; Heyd, J. J.; Brothers, E. N.; Kudin, K. N.; Staroverov, V. N.; Keith, T. A.; Kobayashi, R.; Normand, J.; Raghavachari, K.; Rendell, A. P.; Burant, J. C.; Iyengar, S. S.; Tomasi, J.; Cossi, M.; Millam, J. M.; Klene, M.; Adamo, C.; Cammi, R.; Ochterski, J. W.; Martin, R. L.; Morokuma, K.; Farkas, O.; Foresman, J. B.; Fox, D. J. *Gaussian 16*, Rev. C.01: Wallingford, CT, 2016.